ORIGINAL RESEARCH ARTICLE

DOI: https://doi.org/10.18599/grs.2018.2.58-66

The Unified Scale of Natural Waters

V.F. Nikolaev[1], L.E. Foss[2], B.F. Sulaiman[1], A.B. Agybay[1], A.Kh. Timirgalieva[1], R.B. Sultanova[1]*

[1]*Kazan National Research Technological University, Kazan, Russian Federation*

[2]*Arbuzov Institute of Organic and Physical Chemistry, FRC Kazan Scientific Center of RAS, Kazan, Russian Federation*

Abstract. The article presents a continual scale of natural waters based on the characteristics of a vector, constructed on the superimposed cationic and anionic Gibbs triangles. We made a stylized hydrochemical clock-type dial based on the compression data of a six-component ionic composition of waters. To ensure successful communication of hydrochemists, exchanging information, we suggest characterize the mineral composition of waters by the direction of the vector, expressed in units (minutes) of the hydrochemical clock-type dial. The article presents equations for digitizing natural waters and for color visualization on hydrogeochemical maps of their mineral composition using Red/Green/Blue and Hue/Saturation/Value models. The analysis of the changes occurring in the natural water composition on maps in time enables us to visually establish hydrodynamic connections between ocean currents, water-bearing horizons, oil reservoirs, producing and injecting wells without using tracers. We provide examples of how the six-component composition of the natural waters of lakes, rivers, seas and oceans transforms into indicators of the hydrochemical clock-type dial and the corresponding color tones. The use of the color mapping method to analyze the World Ocean processes, associated with the Arctic ice thawing and changes in the waters composition of ocean currents, will allow us to take a fresh look at the global processes of climate change.

Keywords: natural waters, ground waters, seawaters, ocean currents, reservoir waters, water classification, cationic composition, anionic composition, analytical chemistry, physical chemistry, mineralization, geochemical map, Gibbs-Roseboom triangle, Maxwell triangle, hydrogeochemistry, HSV (HSB) color model, RGB model, horizontal hydrogeochemical zoning, vertical hydrogeochemical zoning, oil and gas field, data compression

Recommended citation: Nikolaev V.F., Foss L.E., Sulaiman B.F., Agybay A.B., Timirgalieva A.Kh., Sultanova R.B. (2018). The Unified Scale of Natural Waters. *Georesursy = Georesources*, 20(2), pp. 58-66. DOI: https://doi.org/10.18599/grs.2018.2.58-66

The diversity of the natural waters composition in six basic ionic components significantly complicates their typification and limits the possibility of "coloring" them in color mapping. In order to partially bypass this obstacle, the waters, marked on the hydrochemical map, are divided into color groups by means of cluster analysis (Narany et al., 2014). The shortcoming of these methods, such as partitioning of waters in the well-known Palmer and Sulin classifications (Palmer, 1911; Sulin, 1946; Collins, 1975; Samarina, 1977; Sulin, 1948), is the discrete character of the boundaries of natural water types, which is incompatible with the continual scales of HSV (HSB) and RGB (Ibraheem et al., 2012; Meskaldji et al., 2009) color models. It is impossible to use the known methods to visualize the six-component composition of natural waters on the Gibbs ionic triangles and to employ the variations of these methods (Žaporozec, 1972) to color hydrogeochemical maps. To date, regional hydrogeochemical maps have been based on the data with one single parameter, for example: total mineralization (*Total Dissolved Solids – TDS*), or the content of chloride ion, sulfate ion or calcium ion (Fraser, 2003). As a result of such mapping, we lose a significant part of the information about the six-component composition of water. Another way of representing natural waters on hydrochemical maps is to draw circular diagrams at the geographical sampling points, the sectoral areas of which reflect the content of the six major ionic components using an equivalent-percent, while the total mineralization of the waters is reflected by the radius of the diagram (Hem, 1985; Dinka et al., 2015). A visual analysis of such maps is also complicated, failing to provide a visual representation of the mineral components migration in water streams.

We used the procedure of data compression by means of a six-component ionic composition represented by points on the cationic (Ca^{2+}, Na^{+}/K^{+}, Mg^{2+}) and anionic (Cl^{-}, SO_4^{2-}, HCO_3^{-}) Gibbs triangles to create a scale of natural waters and their color visualization on hydrogeochemical maps. As shown by the analysis of the experimental data (Collins, 1975; Samarina,

* *Corresponding author: Lev E. Foss*
E-mail: iacw212@gmail.com

1977; Warner et al., 2012), the area of these triangles is extremely unevenly populated because of the low solubility of a number of salts (e.g, calcium sulfate $CaSO_4$, magnesium hydrogen carbonate $Mg(HCO_3)_2$, calcium hydrogen carbonate $Ca(HCO_3)_2$). Due to the low population in the center of ionic triangles, it is possible to use this point to create the scale of natural waters as a center of two auxiliary coordinate systems – Cartesian and polar. The procedure of compressing the data of the six-component water composition involves choosing the optimal way for combining the vertices of the cation and anion triangles, which provides good separation of location of soft water points or vectors (rivers, lakes) and highly mineralized natural waters (sea, ocean, oil-field waters).We did not consider the orientation variants of the anionic triangle with respect to the cationic triangle by rotation to an angle multiple of π/3 (like the six-pointed star of David) because of the possibility of complete mutual compensation of the cation and anion vectors upon their summation.

Having analyzed the compositions of lake, river, sea and ocean waters, given in article (Samarina, 1977), as well as the compositions of the reservoir waters of oil fields (Dresel et al., 2010; Khisamov et al., 2009), we determined that Mg^{2+}/Cl^-, Ca^{2+}/HCO_3^- и $(Na^+/K^+)/SO_4^{2-}$ was the preferred combination of the vertices of the cation and anion triangles. For better perception of the hydrochemical scale, the latter was presented in the form of a regular clock-type dial with sixty divisions and a minute hand, varying in length. The choice of the method for combining the superimposed ionic triangle with the scale of a clock-type dial was made to provide the position of the slightly water-insoluble $Mg(HCO_3)_2$ salt at the beginning of the circular scale (at $\tau_S = 0'$), and position $CaCl_2$ salts with maximum solubility at the end of the scale (at $\tau_S = 60'$). In addition, it was desirable that the remaining salts of natural waters should also be located on the hydrochemical clock-type dial when moving from $\tau_S = 0'$ clockwise in accordance with their increasing solubility in water. The orientation, shown in Figure 1, meets this requirement.

Figure 1 shows that practically all the salts (with the exception of $Ca(HCO_3)_2$) are located on the hydrochemical clock-type dial in accordance with their increasing solubility in water (Kaltofen et al., 1966; Lide, 2006).

The position of a certain sample of natural water on the scale of the hydrochemical clock-type dial can easily be graphically determined by marking the data of cation and anion composition on the superimposed triangle (Figure 1), plotting cationic and anionic vectors, their graphical summation and determining the magnitude τ_S on the hydrochemical scale. Further, we describe in detail the algorithm for computer processing of the hydrochemical information. The following sequence

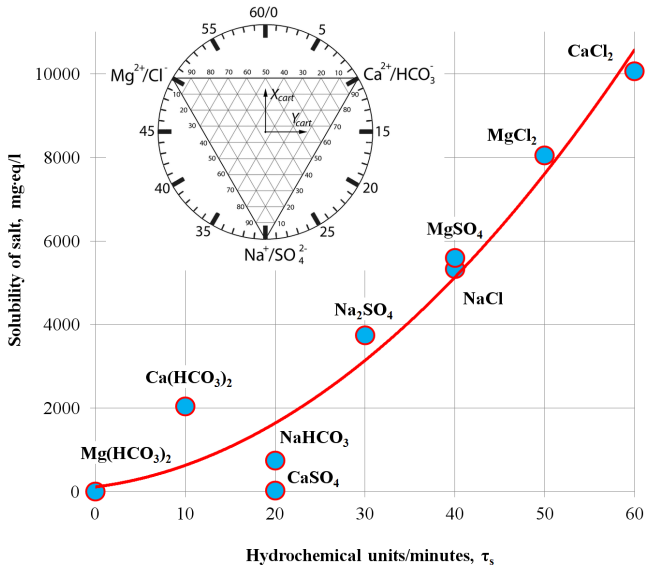

Figure 1. The relationship of solubility of the main individual salt components of natural waters with their position τ_S on the hydrochemical clock-type dial

of coordinate transformations is performed using the chosen mutual orientation of the ionic triangles and the hydrochemical clock-type dial (Figure 1):

$$(X_{GIBBS}; Y_{GIBBS}) \rightarrow (X_{CART}; Y_{CART}) \rightarrow (\varphi; \rho) \rightarrow$$
$$\rightarrow (\varphi'; \rho) \rightarrow (\tau; \rho), \quad (1)$$

where X_{GIBBS} and Y_{GIBBS} are data from a six-component analysis of a certain sample of natural water, meq% (Table 1), X_{CART} and Y_{CART} are the coordinates of the water composition point in the auxiliary Cartesian coordinate system (Figure 1), $\varphi(-180^o<\varphi<+180^o)$ and ρ are the polar coordinates of the radius-vector radiating from the center of the ionic triangle to the point (X_{CART}; Y_{CART}), $\varphi'(0^o<\varphi'<360^o)$ and ρ – are the polar coordinates of the radius-vector with shifted polar angle via clockwise to 180º ($\varphi'=\varphi+180^o$), τ and ρ are the polar coordinates of the radius-vector on the hydrochemical dial scale ($\tau=\varphi'/6$, $0\le\tau\le60$ *min*). Below, we provide specific equations for the transformation of coordinates.

$$X_{GIBBS} = \frac{X_{GIBBS}(Ca^{2+}) + X_{GIBBS}(HCO_3^-)}{2}, \quad (2)$$

$$Y_{GIBBS} = \frac{Y_{GIBBS}(Na^{+}) + Y_{GIBBS}(SO_4^{2-})}{2}. \quad (3)$$

We no longer need the third coordinate $Z_{GIBBS} = [Z_{GIBBS}(Mg^{2+}) + Z_{GIBBS}(Cl^-)]/2$, because by the normalization condition it is uniquely determined by the two used coordinates $Z_{GIBBS} = 100 - X_{GIBBS} - Y_{GIBBS}$.

The coordinates of the superimposed Gibbs triangle (X_{GIBBS}; Y_{GIBBS}) are converted into Cartesian coordinates (X_{CART}; Y_{CART}) using the Eq. (4), (5). The directions of the axes are shown in Figure1.

$$X_{cart} = (100 - Y_{GIBBS}) \cdot \cos\left(\frac{\pi}{6}\right) - 100 \cdot \sin\left(\frac{\pi}{3}\right) + \frac{50}{tg\left(\frac{\pi}{3}\right)}, \quad (4)$$

$$Y_{cart} = (2 \cdot X_{GIBBS} + Y_{GIBBS} - 100) \cdot \cos\left(\frac{\pi}{3}\right). \quad (5)$$

We calculated the direction of the natural water radius-vector in scale units of the hydrochemical clock-type dial by the equation:

$$\tau = 30 \cdot \left(\left(1 - sign\left(30 \cdot \frac{atan2(Xcart;Ycart)}{\pi} - \right.\right.\right.$$
$$\left.\left.\left. - 0.00001\right)\right) + \frac{atan2(Xcart;Ycart)}{\pi}\right), \quad (6)$$

and the length of the normalized radius of the vector is calculated according to the equation:

$$\rho = \sqrt{Xcart^2 + Ycart^2}. \quad (7)$$

Table 1 presents a calculation of the mineral composition characteristics of 21 natural waters. Since after compressing, the data of the six-component composition have been normalized by Eq. (2) and (3), then ρ_S, calculated from Eq. (7) in Table 1, is half the value of ρ_S shown in Figure 2. The given algorithm for calculating the direction and length of the natural waters radius-vector allows us to systematize all natural waters according to the direction τ_S and the length of the radius-vector ρ_S. The subscripts S, A and C at τ, ρ and ρ^{max} mean that the latter values refer to the salt composition of the water, to the anionic composition and to the cationic composition, respectively. By parameter τ_S river waters are located mainly in the range of 5 ÷ 18 units, while sea and ocean waters lie in the range of 35 ÷ 50 units (see τ_S in table 2). A useful addition to the characterization of the water composition is the value $\tau_S \cdot \rho_S / \rho_S^{max}$ which is a derivative from the obtained characteristics of the position of the mineral water composition vector on the hydrochemical clock-type dial, where ρ_S^{max} is the distance from the center of the clock-type dial to the edge of the ionic triangle for the particular direction τ, calculated from equation:

$$\rho^{max} = 50 \cdot \frac{tg\left(\frac{\pi}{6}\right)}{cos\left(\left(abs(abs(abs(\tau - 30) - 20) - 10)\right) \cdot \frac{\pi}{30}\right)}. \quad (8)$$

Using the value $\tau \cdot \rho / \rho^{max}$, we obtain an additional criterion for characterizing the water composition. According to this criterion, lake and river waters come within the range of $\tau_S \cdot \rho_S / \rho_S^{max} = 1 \div 10$, while sea and oceanic waters and reservoir waters of oil and gas fields are found in the range of $\tau_S \cdot \rho_S / \rho_S^{max} = 25 \div 40$.

Digitization of compression data on the composition of natural waters for hydrogeochemical mapping using HSV(HSB) and RGB models

HSV(HSB) color model

For color visualization of changes in the mineral composition of natural waters on the hydrogeochemical maps, we used the data compression procedure for the six-component composition described above and the HSV color model (Hue/Saturation/Value (or Brightness), in which the first position (Hue) changes within the range 0 ÷ 360°, while the second (Saturation) and the third (Value/Brightness) positions change within the interval 0 ÷ 100%. The previously determined characteristics of the vector $\bar{\rho}_S$ position on the hydrochemical clock-type dial and the position of Hue create a circular color scale from the red through yellow, green, blue to purple color. It is only natural that the position of the Hue should be related to the direction τ_S of the natural water total vector $\bar{\rho}_S = \bar{\rho}_C + \bar{\rho}_A$ on the hydrochemical clock-type dial (Figure 2). In the simplest case, if the waters marked on the map cover almost the entire scale of the hydrochemical clock-type dial $\tau_S = 0 \div 60'$, then the Hue value can be calculated as Hue = $6 \cdot \tau_S$. According to the HSV color model, the color circle, surrounding the hydrochemical clock-type dial, has a maximum in the red region of the spectrum (palette) at the point of Hue = 0/360° ($\tau_S = 0/60'$). For the purpose of a more precise color separation, hydrochemical maps of low mineralized lacustrine and river waters lying, with exception of Nile and Yellow River, in the interval $\tau_S = 5 \div 18'$, and highly mineralized sea, oceanic and formation (underground) waters, it is desirable to perform a minute-wise rotation of the color circle by 10′ relative to the clock-type dial. This procedure allows us to color red to yellow all low mineralized and fresh waters of lakes and rivers in the warm part of the spectrum, as for highly mineralized sea, oceanic and reservoir waters, located in the sector $\tau_S = 35 \div 50'$,

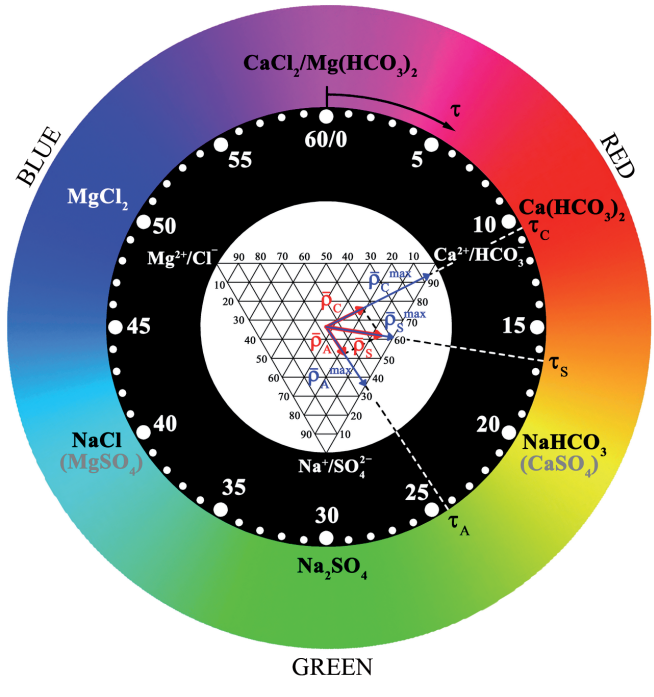

Figure 2. The hydrochemical clock-type dial (HSV model, Hue = 6·(τ$_S$ – 10)) with superimposed triangles of cationic and anionic composition and a graphic example of determining the characteristics of the hydrochemical vector for the water from the Thames River (UK) (Table 1)

we color them in cold colors from blue to purple. Analytically, this rotation of the color circle relative to the clock-type dial by 10′ is expressed by the equation:

$$Hue = 6 \cdot \left(\tau - 10 + 60 \cdot TRUNC\left(\frac{60-\tau}{50}\right)\right), \quad (9)$$

where TRUNC is the Microsoft Office Excel function. Equation (9) is used to form a column of colors (Table 2).

As will be shown below, such ten-minute shift of the colored circle relative to the clock-type dial ensures the similarity of the water color in the HSV (HSB) model to that of the RGB model (Maxwell triangle).

If the waters marked on the hydrogeochemical map have a narrow variation range τ_S, the color scale can be selected (Figure 3) by means of a linear transformation:

$$Hue = \frac{A \cdot (\tau_S - \tau_S^{min})}{(\tau_S^{max} - \tau_S^{min})} + B, \quad (10)$$

where A, B are constants selected from the range $(A + B) \leq 360$, τ_S is the direction of the water sample vector ρ_S on the hydrochemical clock-type dial, τ_S^{min}, τ_S^{max} are the minimum and maximum values of the directions of the water vectors. In order to ensure purity and saturation of colors, the position of the Saturation when forming a column of colors in Table 2 was equaled to the maximum value S = 100%, although other variants are possible. Another reason for not using all the three positions of the HSV (HSB) model is the difficulty of presenting a 3-dimensional decoding of the used color symbols on the plane of the map.

It is logical to connect the Value/Brightness position of the HSV (HSB) model with the distance of the water point to the center of the superimposed triangle ρ. However, the use of this parameter requires its preliminary normalization with respect to the maximum length of the radius-vector ρ_S^{max} for a given one τ_S, i.e. the value ρ_S/ρ_S^{max} that was used in the calculation of Eq. (11). We used the total mineralization of M_S (mEq/L or g/L) in the second variant (12) of calculating the parameter Value. To ensure the purity of the color (Table 2) and its recognizability at high brightness, we used only a narrow range of Value = 50 ÷ 80. There are three variants of equations (11)-(13) for calculating the magnitude of Value:

No*	Ca^{2+}	Na^+/K^+	Mg^{2+}	HCO_3^-	SO_4^{2+}	Cl^-	M	lnM	τ_C	ρ_C	ρ_C^{max}	$\frac{\rho_C}{\rho_C^{max}}$
	meq%			meq%			mEq/L					
1	44.07	14.97	40.95	52.53	27.62	19.85	14.3	2.661	0.9	16.0	29.0	0.551
2	26.68	29.35	43.98	75.77	10.29	13.94	8.2	2.103	10.2	23.2	56.0	0.414
3	54.66	21.92	23.43	67.10	16.16	16.73	2.7	1.006	9.6	18.5	54.0	0.343
4	91.04	6.64	2.33	86.81	4.37	8.82	12.0	2.487	10.4	50.0	53.8	0.930
5	75.73	13.33	10.94	64.78	18.19	17.03	13.3	2.587	10.3	36.7	54.7	0.672
6	64.05	15.95	20.00	89.58	9.40	1.02	2.5	0.905	9.3	26.7	51.2	0.521
7	73.49	14.33	12.18	71.19	18.11	10.69	10.1	2.311	10.3	34.8	54.8	0.635
8	34.53	46.49	18.98	67.97	15.35	16.68	2.6	0.956	24.3	13.8	32.0	0.431
9	44.94	30.27	24.79	50.91	40.63	8.46	12.4	2.518	12.5	10.4	40.6	0.256
10	54.30	24.11	21.59	34.23	46.79	18.98	16.0	2.770	10.7	18.2	51.6	0.352
11	3.80	88.68	7.51	59.39	0.33	40.28	321.7	5.773	30.4	48.0	54.1	0.886
12	3.93	44.41	51.66	4.12	91.77	4.11	942.9	6.849	41.4	25.7	29.2	0.882
13	8.69	62.88	28.43	0.64	29.36	70.00	431.5	6.067	33.5	27.4	37.1	0.739
14	3.43	79.62	16.95	0.28	10.59	89.14	1386.6	7.235	31.6	40.7	45.3	0.897
15	3.32	79.11	17.57	1.05	9.11	89.85	1401.1	7.245	31.7	40.3	44.7	0.900
16	4.04	78.34	17.62	1.04	9.28	89.68	600.9	6.398	31.6	39.6	45.0	0.879
17	3.35	78.73	17.92	0.38	9.28	90.34	1250.5	7.131	31.8	40.0	44.4	0.900
18	29.55	41.81	28.64	31.74	25.68	42.57	97.8	4.583	29.4	7.4	52.2	0.141
19	25.15	69.05	5.80	0.03	0.00	99.96	7014.2	8.856	27.1	32.4	39.2	0.826
20	13.07	32.41	54.53	0.17	0.06	99.76	12761.6	9.454	45.4	20.7	34.1	0.608
21	41.52	34.27	24.22	26.98	21.23	51.79	17.6	2.869	15.9	8.7	31.8	0.273

Table 1. A content of natural waters and characteristics of cationic component on dial.
**Numbers are the following water samples: 1) Southwestern Ontario's Breathing Well Region. Canada (Freckelton, 2012); 2) Volga river. Russia (Fraser, 2003); 3) Freshwater (typical ions) (Bortman et al., 2003); 4) Lambourn river, UK (Allen at al., 2010); 5) Seine river, France (Fraser, 2003); 6) Baikal Lake. Russia (Fraser, 2003); 7) Elbe river, Czech Republic (Ritter et al., 2011); 8) Severn river,UK (Shand et al., 2005); 9) Missouri river, USA (Criss et al., 2001); 10) Thames river basin, UK (Bearcock et al., 2010); 11) Yessentuki 17, mineral water, Russia (Samarina, 1977); 12) Hunyadi János, mineral water, Hungary (Halaj,2013); 13) Caspian Sea (Fraser, 2003); 14) Red Sea (Manheim et al., 2007); 15) Mediterranean sea (Demirel et al., 2006); 16) Black Sea (Schug, 2003); 17) Ocean (typical ions) (Bortman et al., 2003); 18) Nile river, Egypt (Hossam, 2010); 19) Pennsylvania brine water, USA (Dresel et al., 2010); 20) Dead Sea (Lopatina,2016); 21) Yellow river, China (Jing et al., 2014).*

No*	τ_A	ρ_A	ρ_A^{max}	$\frac{\rho_A}{\rho_A^{min}}$	τ_S	$\tau_{S\text{-}10}$	Hue	ρ_S	ρ_S^{max}	Value	$\frac{\rho_S}{\rho_S^{max}}$	$\tau_S \cdot \frac{\rho_S}{\rho_S^{max}}$	Color HSV
1	12.19	17.08	42.22	0.404	6.77	56.8	341	13.7	38.0	74	0.361	2.45	
2	14.53	20.70	34.36	0.602	7.26	57.3	344	21.4	42.1	76	0.508	6.21	
3	9.91	29.25	56.78	0.515	9.79	59.8	359	23.9	55.6	80	0.429	4.20	
4	9.54	46.37	53.37	0.869	9.99	60.0	360	48.1	57.7	74	0.835	8.34	
5	10.20	27.24	55.70	0.489	10.26	0.3	2	32.0	55.1	74	0.580	5.96	
6	10.82	48.89	50.43	0.969	10.27	0.3	2	37.7	55.0	80	0.685	7.03	
7	11.08	33.00	48.58	0.679	10.68	0.7	4	33.9	51.6	75	0.657	7.01	
8	9.79	30.00	55.61	0.539	13.81	3.8	23	16.8	36.2	80	0.465	6.42	
9	17.76	22.15	29.68	0.746	16.11	6.1	37	15.8	31.4	74	0.501	8.08	
10	24.47	13.93	32.34	0.431	16.45	6.5	39	12.1	31.0	73	0.391	6.44	
11	3.08	30.14	30.44	0.990	26.38	16.4	98	10.4	36.8	63	0.283	7.47	
12	30.00	50.61	57.72	0.877	33.60	23.6	142	32.4	36.8	59	0.879	29.54	
13	45.94	34.85	35.53	0.981	40.59	30.6	184	24.9	28.9	62	0.860	34.91	
14	48.99	48.60	49.01	0.992	41.38	31.4	188	27.6	29.2	58	0.944	39.08	
15	49.22	49.11	50.70	0.969	41.68	31.7	190	27.4	29.3	58	0.935	38.95	
16	49.20	48.98	50.55	0.969	41.74	31.7	190	27.1	29.4	61	0.924	38.56	
17	49.14	49.57	50.14	0.989	41.75	31.8	191	27.7	29.4	58	0.944	39.42	
18	53.46	8.56	37.28	0.229	43.63	33.6	202	2.5	31.1	67	0.081	3.52	
19	50.00	57.70	57.71	1.000	44.51	34.5	207	20.2	32.4	52	0.622	27.70	
20	50.01	57.53	57.64	0.998	48.80	38.8	233	38.2	47.7	50	0.801	39.11	
21	51.70	16.24	44.73	0.363	56.46	46.5	279	5.2	31.0	73	0.168	9.46	

Table 2. The positions of anionic and salt components of natural waters on dial.
**Denotation of water samples see Table 1*

$$Value(Brightness) = 80 - 30 \cdot \frac{\rho}{\rho^{max}}, \quad (11)$$

$$Value(Brightness) = 80 - 30 \cdot \frac{(M_{Si} - M_S^{min})}{(M_S^{max} - M_S^{min})}. \quad (12)$$

In the case of hydrochemical mapping when the waters differ significantly in total mineralization, we can use the logarithm of total mineralization lnM_s as in Eq. (13) instead of Eq. (12):

$$Value(Brightness) = 80 - 30 \cdot \frac{(lnM_{Si} - lnM_S^{min})}{(lnM_S^{max} - lnM_S^{min})}. \quad (13)$$

Table 2 shows examples of conversion of the natural waters composition into color (Hue is calculated by Eq. (9), Saturation = 100%, Value is calculated by Eq. (13)).

The approach, representing the mineral composition of waters with the values τ_S and ρ_S in the HSV model, is fully implemented in the construction of hydrogeochemical maps only in the case of the cationic or anionic components of the waters, if we replace τ_S with τ_C or τ_A, and ρ_S/ρ_S^{max} with ρ_C/ρ_C^{max} or ρ_A/ρ_A^{max}, respectively. The same relationships (4)-(9) are valid for the calculation of τ_C, ρ_C, ρ_C^{max}, τ_A, ρ_A, ρ_A^{max} parameters, only if $X_{GIBBS}(Ca^{2+})$, $Y_{GIBBS}(Na^+)$ and $X_{GIBBS}(HCO_3^-)$, $Y_{GIBBS}(SO_4^{2-})$ are used in equations (4) and (5) instead of X_{GIBBS} and Y_{GIBBS} for cations and anions respectively.

RGB color model. Combined Gibbs-Maxwell triangle

The RGB (Red / Green / Blue) is a second model, used for color visualization of various geological and hydrogeochemical characteristics of territories in mapping. The positions R, G and B vary in the range from 0 to 255 (Ibraheem et al., 2012). It is possible to transfer the coordinates of the superimposed cation-anion triangle of Gibbs composition to Maxwell's color triangle (14) due to the earlier compression of the data of the six-component water analysis by Eq. (2)-(3):

$$(X_{GIBBS}, Y_{GIBBS}) \rightarrow (x; y) \rightarrow (x; y; 1 - x - y) \rightarrow$$
$$\rightarrow (r; g; b) \xrightarrow{Maxwell} RGB. \quad (14)$$

The coordinates of the waters on the superimposed Gibbs triangle are equated with the coordinates of the Maxwell triangle (equations (15)-(17)) to achieve color visualization of the mineral composition of natural waters on hydrogeochemical maps:

$$x(Ca^{2+}/HCO_3^-) = \frac{X(Ca^{2+}/HCO_3^-)}{100} = r = \frac{R}{R+G+B}, \quad (15)$$

$$y(Na^+/SO_4^{2-}) = \frac{Y(Na^+/SO_4^{2-})}{100} = g = \frac{G}{R+G+B}, \quad (16)$$

$$z(Mg^{2+}/Cl^-) = \frac{Z(Mg^{2+}/Cl^-)}{100} = b = \frac{B}{R+G+B}, \quad (17)$$

where *r, g* and *b* are the color coordinates on the Maxwell triangle in the RGB model.

The examples of the transformation of the Gibbs coordinates for 21 natural waters into the Maxwell color RGB triangle are given in Table 3. The waters are arranged in Table 3 as τ_S grows. The hydrochemical clock-type dial shows that the color tones of river and lake waters are

No*	Gibbs triangle compressed coordinates			Coordinates of Maxwell triangle			Color
	$x(Ca^{2+}/HCO_3^-)$	$y(Na^+/SO_4^{2-})$	$z(Mg^{2+}/Cl^-)$	R	G	B	
1	0.483	0.213	0.304	255	112	160	
2	0.512	0.198	0.290	255	99	144	
3	0.609	0.190	0.201	255	80	84	
4	0.889	0.055	0.056	255	16	16	
5	0.703	0.158	0.140	255	57	51	
6	0.768	0.127	0.105	255	42	35	
7	0.723	0.162	0.114	255	57	40	
8	0.513	0.309	0.178	255	154	89	
9	0.479	0.355	0.166	255	189	88	
10	0.443	0.355	0.203	255	204	117	
11	0.316	0.445	0.239	181	255	137	
12	0.040	0.681	0.279	15	255	104	
13	0.047	0.461	0.492	24	239	255	
14	0.019	0.451	0.530	9	217	255	
15	0.022	0.441	0.537	10	209	255	
16	0.025	0.438	0.537	12	208	255	
17	0.019	0.440	0.541	9	207	255	
18	0.306	0.337	0.356	219	242	255	
19	0.126	0.345	0.529	61	166	255	
20	0.066	0.162	0.771	22	54	255	
21	0.342	0.277	0.380	230	186	255	

Table 3. Coordinates of natural waters on the Gibbs and Maxwell triangles.
**Denotation of water samples see Table 1*

characterized by either warm color or low color intensity (the River Nile in Egypt and the River Yellow in China) on the combined Gibbs-Maxwell triangle.

As shown above, the algorithms used for transferring the data of the six-component waters composition to color by means of the HSV and RGB models are fully applicable to the construction of individual hydrogeochemical maps only in the case of the cationic or anionic components.

A simplified example for color mapping of changes in mineral composition of reservoir waters of oil and gas field in Surfer program (Ozler, 2003)

We prepared color map using the Surfer software (Ozler, 2003). Figure 3 shows a schematic example of a hydrogeochemical chart based on the data on the six-component composition and total mineralization of the reservoir waters in oil and gas fields of Western Pennsylvania (Dresel et al., 2010). To create the map we used the well data with a virtually overlapping perforation depth range.

It shows the mineral composition of the reservoir waters. You can see that against the background of the main mineral component of NaCl, formation waters have a high content of calcium chloride $CaCl_2$ in the blue-colored area in contrast to other areas of the map, painted in red, yellow and green colors τ_S (NaCl)=40′ corresponds to the aqueous solution of pure sodium chloride while τ_S ($CaCl_2$)=60′ corresponds to the pure aqueous solution of calcium chloride. It should be noted that $MgCl_2$ at τ_S ($MgCl_2$) = 50′ is found on the hydrochemical scale τ_S between NaCl and $CaCl_2$; however, in this case, the displacement of the reservoir waters of the West Pennsylvania field is connected with an increase in the $CaCl_2$ content, which has τ_S ($CaCl_2$)=60′.

The proposed method of analyzing hydrochemical information about reservoir waters in oil fields will allow us, in certain cases, to reject tracer methods of determining hydrodynamic connections between strata and between producing and injection wells, since natural components of formation and injected waters can act as distinct tracers. The color similarity of waters on the hydrogeochemical map will also mean the similarity of their mineral composition, which in turn will indicate the presence of a hydrodynamic connection between water streams, horizons (strata) or wells. This method can be used in visual analyses of data both on horizontal (areal) and vertical (deep) hydrogeochemical zoning of oceanic and sea waters as well as waters of oil and gas fields. Color visualization of changes in the mineral composition of formation water can be carried out in the absence of data on the six-component analysis. It is sufficient to determine only its two characteristics – their refractive index n_D^{20} and density d^{20} (g/cm^3), and use the algorithm described in our article (Nikolaev et

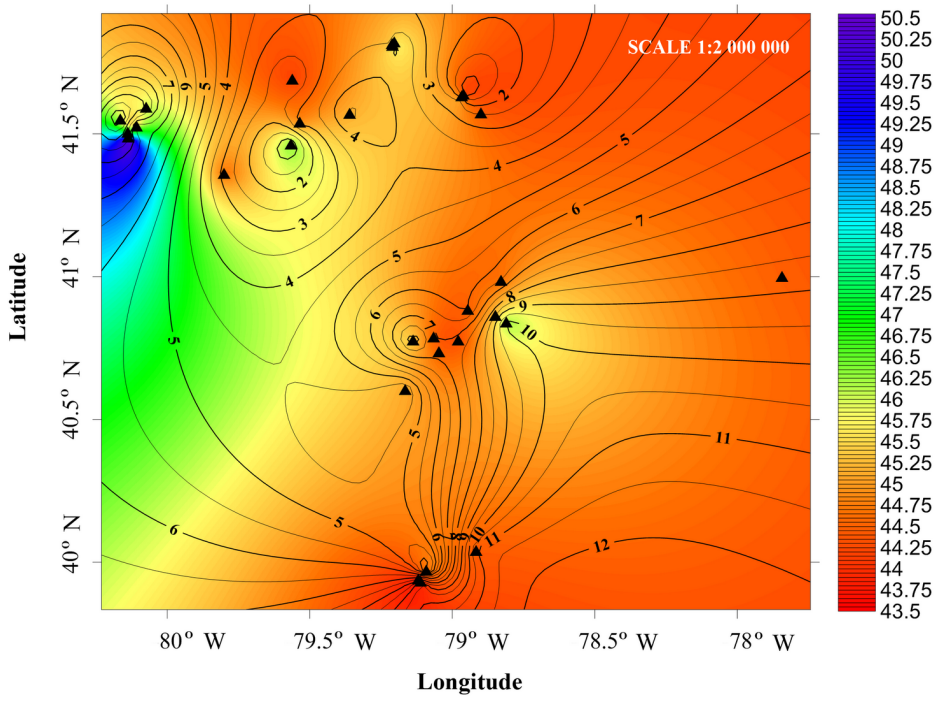

Figure 3. A schematic hydrogeochemical map of oil and gas province of Western Pennsylvania created with the SURFER software package and with the use of the values τ_S (color) and the logarithms of total mineralization lnM (M, mEq/L) (isolines)

al., 2016). To select the color (tone), we should use the identification polar angle φ_{IPA}, and the polar radius ρ as a measure of total mineralization (Nikolaev et al., 2018).

The described method of compression and digitization of analytical information can be used in color visualization of various mass transfer processes, as it groups individual components of a multicomponent system in accordance with some unifying property and presents a real multicomponent system of a composition changing in space and time as a form of a pseudo-ternary system, like the one used in analyzing light petroleum products and motor fuels (Nikolaev, 2015; Nikolaev, 2012). On the color petrogeochemical maps of oil fields, the change in the content of oils can be visualized by compressing the 4-component oil composition data, determined by the SARA analysis (ASTM D4124-09), up to a 3-component composition by allocating a saturated hydrocarbon group, an aromatic hydrocarbon group and a combined group of resins and asphaltenes.

Conclusion

We propose a continual circular hydrochemical scale (clock-type dial) of natural waters τ_S, based on the compression of data on their six-component ionic composition. A conventional agreement on a uniform method for compressing data on a six-component composition of natural waters, and a method for displaying it on a hydrochemical clock-type dial adopted by the International Association of Hydrogeologists (Hydrology) will facilitate the communication of hydrologists and hydrochemists in exchanging information.

The hydrochemical clock-type dial as a showing part of the device can be placed on the navigational instrument panel of sea and river vessels when used in developing a rapid method for determining the six-component composition of natural waters in the future.

Owing to the continuity of the hydrochemical scale, the results of digitizing the mineral composition of waters are well compatible with the HSV and RGB color models widely used in geochemical mapping. We demonstrate the effectiveness of combining the Gibbs ionic composition triangle and Maxwell's color triangle into a single Gibbs-Maxwell triangle in the case of using the RGB model.

By implementing the method of color visualization of the water mineral composition we can optimize the development of oil and gas fields. We can also conduct retrospective analyses of large volumes of hydrogeochemical and petroleum geochemical information, accumulated in laboratories of oil companies throughout the years of development and operation of oilfields. Of special interest is the information on the changes in hydrodynamic interactions between oil reservoirs, water horizons, producing and injection wells. In order to better visualize hydrodynamic connections between the injection and production wells, waters can be used instead of injecting tracers. These waters differ from natural reservoir waters either in their mineral composition or in their total mineralization. However, their mutual compatibility is required.

References

Allen D.J., Darling W.G., Gooddy D.C., Lapworth D.J., Newell A.J., Williams A.T., Allen D., Abesser C. (2010). Interaction between groundwater, the hyporheic zone and a Chalk stream: a case study from the River Lambourn. UK. *Hydrogeology*, 18, pp.1125-1141.

Bortman M., Brimblecombe P., Cunningham M.A., Cunningham W.P., Freedman W. (2003). Environmental Encyclopedia. Gale, Farmington Hills.

Bearcock J.M., Smedley P.L. (2010). Baseline groundwater chemistry: the Palaeogene of the Thames Basin. British Geological Survey Open Report, OR/10/057. http://nora.nerc.ac.uk/12600/1/OR10057.pdf

Collins A.G. (1975). Developments in Petroleum Science. Vol. I. *Geochemistry of Oilfield Waters*, Elsevier Science, New York, 496 p.

Criss R.E., Davidson M.L., Kopp J.W. (2001). Nonpoint sources in the lower Missouri River. *Am. Water Works Assoc*., 93, pp. 112-122.

Dinka M.O., Loiskandl W., Ndambuki J.M. (2015). Hydrochemical characterization of various surface water and groundwater resources available in Matahara areas, Fantalle Woreda of Oromiya region. *Journal of Hydrology: Regional Studies*, 3, pp. 444-456.

Dresel P.E., Rose A.W. (2010). Chemistry and Origin of Oil and Gas Well Brines in western Pennsylvania, Open-File Oil and Gas Report 10-01.0. Pennsylvania geological survey. http://www.fwspubs.org/doi/suppl/10.3996/052013-JFWM-033/suppl_file/patnodereference+s3.pdf

Demirel Z., Güler C. (2006). Hydrogeochemical evolution of groundwater in a Mediterranean coastal aquifer, Mersin-Erdemli basin (Turkey). *Environ Geol.*, 49, pp. 477-487.

Fraser A.S., Ongley E.D., Meybeck M, Hodgson K. (2003). The Annotated Digital Atlas of Global Water Quality, Global environment monitoring system freshwater quality programme, National Water Research Institute. http://colinmayfield.com/biology447/modules/module1/gems/intro.html

Freckelton C.N. (2013). A Physical and Geochemical Characterization of Southwestern Ontario's Breathing Well Region. The University of Western Ontario. https://ir.lib.uwo.ca/cgi/viewcontent.cgi?article=2407&context=etd

Hem J.D. (1985). Study and Interpretation of the Chemical Characteristics of Natural Waters. U.S. Geological Survey Water, United States government printing office, Wasington, 263 p.

Halaj E., Wachowicz-pyzik A. (2013). Examples of applications of geothermal waters for refraction, heating and bottling in selected regions of Hungary. *Geol, Geoph & Environ*, 39, pp. 21-32.

Hossam H.E. (2010). Potentialities of Water Resources Pollution of the Nile River Delta, Egypt. *The Open Hydrology J*., 4, pp. 1-13.

Ibraheem N.A., Hasan M.M., Khan R.Z. (2012). Understanding Color Models: A Review. *Journal of Sci. and Tech*., 2, pp. 265-275.

Jing L., Fadong L., Qiang L., Shuai S., Yan Zh., Guangshuai Z. (2014). Impacts of Yellow River Irrigation Practices on Trace Metals in Surface Water: A Case Study of the Henan-Liaocheng Irrigation Area, China. *Human and Ecolog Risk Assessment: An Inter J.*, 20, pp. 1042-1057.

Kaltofen R., Opitz R., Schumann K., Ziemann J. (1966). Tabellenbuch Chemie. VEB Deutscher Verlag für Grundstoffindustrie, Leipzig, 485 p.

Khisamov R.S., Gabdullin T.G., Farhullin R.G. (2009). Control over the development of oil and gas fields. Idel-Press, Kazan, 408 p. (In Russ.)

Lide D.R. (2006). Concentrative Properties of Aqueous Solutions: Density, Refractive Index, Freezing Point Depression, and Viscosity, in CRC Handbook of Chemistry and Physics. Taylor and Francis. http://www.hbcpnetbase.com

Lopatina A.B. (2016). The chemical composition of the Dead Sea (Israel). *Sci Bull*., 7, pp. 215-221. (In Russ.)

Meskaldji Kh., Boucherkha S., Chikhi S. (2009). Color Quantization and its Impact on Color Histogram Based Image Retrieval. CEUR-WS Publisher. http://ceur-ws.org/Vol-547/60.pdf

Manheim F.T., Waterman L.S., Woo C.C., Sayles F.L. (2007). Deep Sea Drilling Project DSDP Volume XXIII. Interstitial Water Studies on Small Core Samples, Leg 23 (Red Sea). http://www.deepseadrilling.org/23/volume/dsdp23_35.pdf

Narany T.S., Ramli M.R., Aris A.Z., Sulaiman W.A., Juahir H., Fakharian K. (2014). Identification of the hydrogeochemical processes in groundwater using classic integrated geochemical methods and geostatistical techniques, in Amol-Babol Plain, Iran. *The Sci World J*., 2014. pp. 1-15.

Nikolaev V.F., Timirgalieva A.Kh., Barskaya E.E., Egorov A.V., Khanova D.R., Sultanova R.B., Romanov G.V. (2016). Hydrogeochemistry: natural waters in full view. *Bulletin of Kazan Technological University*, 19, pp. 5-10. (In Russ.)

Nikolaev V.F., Tabrisov I.I., Penkovsky A.I., Sultanova R.B. (2015). Express method for total content assessment of aromatic hydrocarbons and oxygen in finished gasolines by refractometry and densimetry. *Fuel*, 142, pp. 94-101.

Nikolaev V.F. (2012). Rapid methods for testing composite products of oilfield chemistry and motor fuels. Kazan, KNRTU, 124 p. (In Russ.)

Nikolaev V.F., Bulygin D.V. (2018). Express Method to Evaluate Mineral Composition of Injected and Associated Water at the Oil Fields. *Oil. Gaz. Novations*, No.4, pp. 48-52.

Ozler H.M. (2003). Hydrochemistry and salt-water intrusion in the Van aquifer, east Turkey. *Environmental Geology*, 43. pp. 759-775.

Palmer C.C. (1911). The geochemical interpretation of water analysis. Government printing office, Washington, 31 p.

Ritter D.J. (2011). First Order Analysis of Nitrate Loading in the Upper Elbe River Basin, Czech Republic. Brigham Young University BYU Scholars Archive. http://scholarsarchive.byu.edu/cgi/viewcontent.cgi?article=3871&context=etd

Samarina V.S. (1977). Hydrogeochemistry. Leningrad, Leningrad State Univ-ty, 360 p. (In Russ.)

Sulin V.A. (1946). Waters of Petroleum Formations in the System of Nature Waters. Moscow, Gostoptekhizdat, 95 p. (In Russ.)

Sulin V.A. (1948). Conditions of formation, the basis of classification and composition of natural waters. Part 1. Moscow, USSR Academy of Sciences, 105 p. (In Russ.).

Shand P., Abesser C., Farr G., Wilton N., Lapworth D.J., Gooddy D.C., Haria A., Hargreaves R. (2005). Baseline Report Series: 17. The Ordovician and Silurian meta-sedimentary aquifers of central and south-west Wales. British Geological Survey. http://nora.nerc.ac.uk/3550/1/CR05034N.pdf

Schug D.M. (2003). Deep Sea Drilling Project DSDP Volume XXIII Interstitial Waters of Black Sea Cores. http://www.deepseadrilling.org/42_2/volume/dsdp42pt2_23.pdf

Warner N.R., Jackson R.B., Darrah T.H., Osborn S.G., Down A., Zhao K., White A., Vengosh A. (2012). Geochemical evidence for possible natural migration of Marcellus Formation brine to shallow aquifers in Pennsylvania *Proceed in Nat. Acad. of Sci.*, 109, pp. 11961-11966.

Žaporozec A. (1972). Graphical Interpretation of Water-Quality Data. *Ground Water*, 10, pp. 32-43.

About the Authors

Vyacheslav F. Nikolaev – DSc (Chemistry), Professor, Department of Technology of Basic Organic and Petrochemical Synthesis

Kazan National Research Technological University
68 Karl Marx str., Kazan, 420015, Russian Federation

Lev E. Foss – PhD, Junior researcher of Oil Chemistry and Geochemistry Laboratory

Arbuzov Institute of Organic and Physical Chemistry, FRC Kazan Scientific Center of the Russian Academy of Sciences

8 Arbuzov str., Kazan, 420088, Russian Federation
E-mail: iacw212@gmail.com

Bassel .F. Sulaiman – PhD Student, Department of Technology of Basic Organic and Petrochemical Synthesis

Kazan National Research Technological University
68 Karl Marx str., Kazan, 420015, Russian Federation

Asel B. Agybay – Master, Department of Technology of Basic Organic and Petrochemical Synthesis

Kazan National Research Technological University
68 Karl Marx str., Kazan, 420015, Russian Federation

Alina Kh. Timirgalieva – Master, Department of Technology of Basic Organic and Petrochemical Synthesis

Kazan National Research Technological University
68 Karl Marx str., Kazan, 420015, Russian Federation

Rasimya B. Sultanova – PhD (Chemistry), Associate professor, Department of Technology of Basic Organic and Petrochemical Synthesis
Kazan National Research Technological University
68 Karl Marx str., Kazan, 420015, Russian Federation

Manuscript received 8 February 2018;
Accepted 23 May 2018;
Published 30 June 2018